Altered development of the brain after focal herpesvirus infection of the central nervous system

Thad Koontz,[1] Marina Bralic,[4] Jelena Tomac,[4] Ester Pernjak-Pugel,[4] Glen Bantug,[3] Stipan Jonjic,[4] and William J. Britt[1,2,3]

[1]Department of Neurobiology, [2]Department of Pediatrics, and [3]Department of Microbiology, University of Alabama at Birmingham, Birmingham, AL 35294
[4]Department of Embryology and Histology, Faculty of Medicine, University of Rijeka, HR-51000 Rijeka, Croatia

The Journal of Experimental Medicine

Human cytomegalovirus infection of the developing central nervous system (CNS) is a major cause of neurological damage in newborn infants and children. To investigate the pathogenesis of this human infection, we developed a mouse model of infection in the developing CNS. Intraperitoneal inoculation of newborn animals with murine cytomegalovirus resulted in virus replication in the liver followed by virus spread to the brain. Virus infection of the CNS was associated with the induction of inflammatory responses, including the induction of a large number of interferon-stimulated genes and histological evidence of focal encephalitis with recruitment of mononuclear cells to foci containing virus-infected cells. The morphogenesis of the cerebellum was delayed in infected animals. The defects in cerebellar development in infected animals were generalized and, although correlated temporally with virus replication and CNS inflammation, spatially unrelated to foci of virus-infected cells. Specific defects included decreased granular neuron proliferation and migration, expression of differentiation markers, and activation of neurotrophin receptors. These findings suggested that in the developing CNS, focal virus infection and induction of inflammatory responses in resident and infiltrating mononuclear cells resulted in delayed cerebellar morphogenesis.

CORRESPONDENCE
William J. Britt:
wbritt@peds.uab.edu

Abbreviations used: BDNF, brain-derived neurotrophic factor; BDV, Borna disease virus; CNS, central nervous system; EGL, external granular neuron layer; GNP, granule neuron precursor; HCMV, human cytomegalovirus; IE, immediate early; IGL, internal granular layer; IHC, immunohistochemical; MCMV, murine cytomegalovirus; ML, molecular layer; MuLV, murine leukemia virus; NT3, neurotrophin 3; PFA, paraformaldehyde; PN, postnatal.

Infections of the developing central nervous system (CNS) represent a significant cause of disease in newborn and young infants and can result in permanent neurological deficits. Neurological dysfunction associated with viral infections of the CNS often exceeds cellular damage directly attributable to virus replication, particularly in the developing CNS. Studies in patients with AIDS dementia and in animal models of nonnecrotizing viral infections of the CNS have suggested that host inflammatory responses contribute to the neurological damage associated with these infections (1, 2). Similar immunopathological mechanisms could contribute to the long-term neurological abnormalities that follow virus infection of the CNS of the developing human fetus (3).

Infection of the developing fetus with human cytomegalovirus (HCMV) results in CNS damage of an estimated 3,000 infants each year in the United States (4, 5). Infection of the fetus follows maternal infection and congenitally (present at birth) infected infants exhibit neurodevelopmental abnormalities ranging from mild deficits in perceptual senses such as hearing loss to profound neurological disease secondary to structural damage including cortical and cerebellar hypoplasia (3, 5–7). Lissencephaly, ventriculomegaly, and periventricular calcifications have been reported in severely affected congenitally infected infants. More recent studies using magnetic resonance imaging have suggested that disorders in brain morphogenesis, including pachygyria and microgyria, could be more frequent than previously appreciated, and up to 50% of affected infants have hypoplasia of the cerebellum (8). Histopathological findings from the brains of autopsied infants include focal areas of reactive mononuclear cells, reactive gliosis, microglial nodules, and less often, widespread damage to the periventricular gray matter (3, 6). Mechanisms of neurological damage in infants with HCMV infection remain undefined in part because observational studies of only a limited number of autopsy studies of infected infants have provided the bulk of information about this infection (3, 6).

Proposed mechanisms of disease include disruption of vascular supply in the developing brain, loss of neural progenitors in the subventricular zone, and disordered cellular positioning secondary to altered cell migration (8–12). The majority of infants do not present with findings of severe structural damage of the CNS, yet a significant percentage of these infected children will have permanent neurological deficits. Imaging studies have suggested that disorders of cellular positioning could account for the neurological abnormalities in some infected infants (8, 9, 13).

The species-specific tropism of HCMV that limits virus replication to cells of human origin has also restricted its study in relevant in vivo and in vitro models. Animal models have provided insight into the pathogenesis of HCMV infection of the CNS (14–19). With the exception of a rhesus macaque model, animal models have used direct intracranial inoculation with CMV almost exclusively to achieve CNS infection. Macaques inoculated intraperitoneally during fetal life develop CNS infection and disease; however, recent studies have used direct intracranial inoculation of fetal macaques to consistently induce CNS infection (18, 19). Results from these studies have shown that rhesus CMV can infect a variety of cell types in the CNS (19). Similarly, intracranial inoculation of murine cytomegalovirus (MCMV) has been used to establish CNS infection in mice (16). There are limitations in the extrapolation of results from models using intracranial virus inoculation to the pathogenesis of CMV infections in the developing CNS of humans. Perhaps the most obvious is that neuroinvasion is via intracranial injection, and the spatial distribution of the ensuing infection does not reflect CNS infection that follows hematogenous spread. Furthermore, direct intracranial injection eliminates host-derived immune responses in peripheral tissue that would develop before spreading to the CNS.

We have developed a mouse model of an HCMV infection of the developing CNS using peripheral inoculation of newborn mice with low titers of MCMV. Our results indicated that virus replication in the liver and presumably the spleen was followed by spread to the brain leading to a widespread non-necrotizing focal encephalitis. A variety of resident cell types of the brain was shown to be infected in vivo, and mononuclear cells could be identified in foci of infection. There was increased expression of mRNA-encoding mediators of innate immune responses, including interferon-stimulated genes and chemokines in brains from infected animals. In addition, there were morphological abnormalities in the cerebella of infected animals, a region of the brain that undergoes extensive postnatal (PN) development in the rodent. These changes were global in nature and, although correlated with virus replication in the CNS, independent of contiguous foci of infection. This finding suggested that a soluble mediator(s) was responsible for the symmetric changes observed in the cerebellum of infected mice. Collectively, our findings argued that focal viral infection and inflammation in the developing human CNS could alter developmental programs required for cellular positioning and/or differentiation in the developing brain and, thus, be responsible for some of the neurological disorders associated with congenital HCMV infections.

RESULTS

MCMV replicates in the brain of newborn mice after peripheral inoculation

Newborn BALB/c mice were inoculated intraperitoneally with 200 PFU of infectious MCMV within 24 h of birth, and brain and liver homogenates were titered on days 2–21 after infection to define the kinetics of virus replication. Virus replication in the liver was detected shortly after infection and reached a peak titer of $\sim 10^5$ PFU per gram of tissue by PN day 10 (Fig. 1 A). Peak titers of virus were detected in the brain on PN day 11 and fell below the limits of detection by PN day 17, suggesting that MCMV replicated initially in peripheral organs such as the liver and then spread to the brain (Fig. 1 A). Comparable results were obtained using quantitative PCR to detect MCMV DNA, although significant amounts of viral DNA were detected in the brain of some mice as early as PN day 5 and on PN day 21 (Fig. 1 B). Similar amounts of virus per gram of tissue were detected in both the brain and liver, indicating that in newborn mice, MCMV productively infected the CNS. Significant amounts of viral DNA were detected in the blood of infected animals beginning on PN day 5, suggesting that virus spread hematogenously to the brain (20).

MCMV infects neuronal and glial cells of the brain and leads to a focal encephalitis

To further characterize the extent of MCMV infection of the brain of newborn animals, we identified virus-infected cells in brain sections using an mAb reactive with the major immediate early (IE)-1 protein of MCMV, pp89 (21). Representative examples from the analysis from >30 infected mice from PN days 8–12 are presented in Fig. 1. Infected cells were detected in different regions of the brain, including the frontal cortex, hippocampus, and cerebellum (Fig. 1, C–F). A variety of cell types was infected such as neurons and astroglial cells, including Bergman glia of the cerebellum (Fig. 1, C–F, and not depicted). Infection was not restricted to one resident cell population, suggesting that there was no specific tropism of MCMV infection for cells of the PN CNS. Moreover, we did not observe a significant loss of a particular resident cell population in the infected brain (not depicted). Finally, virus-infected cells could be detected in the meninges overlying different regions of the brain and infrequently in vascular endothelium (not depicted).

The most characteristic finding of infection of the brain in infected mice was focal involvement in different regions of the brain. Discrete foci of infection containing 3–10 infected cells were present throughout all regions of the brain, and serial sections of brains from >30 animals consistently revealed in excess of 100 such foci of infection in individual brains (Fig. 2 A). Because the analysis of brain infection with immunohistochemical (IHC) methods could have underestimated the extent of infection in these animals, we performed in situ

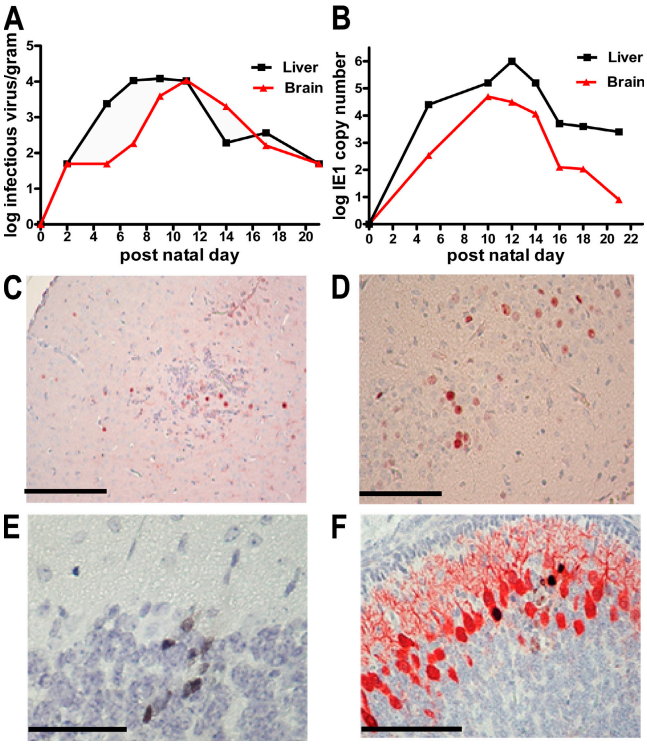

Figure 1. Replication of MCMV in the brains of newborn mice. (A) Virus yield (log) per gram of homogenized liver and brain determined by plaque assay and results expressed as infectious units (PFU)/g of tissue as described previously (reference 21). (B) Real-time PCR performed with MCMV IE-1 primers using DNA extracted from the livers or brains of infected animals as described in Results and Materials and methods, expressed as IE-1 copy number per 200 μl of 10% homogenate as a function of time after infection (reference 77). (C–F) IHC detection of virus-infected cells using anti-pp89 (IE-1) in (C) the frontal cortex from a PN day 12 mouse, (D) in neurons of hippocampus from a PN day 11–infected mouse, (E) granular neurons of cerebellum, and (F) Purkinje neurons of cerebellum from PN day 11 mice. In C and D, the MCMV pp89 is represented by the red signal, and in E it is a black signal. In F, dual staining for calbindin (red) and MCMV pp89 (black) was used to demonstrate cellular localization of viral antigen. Paraffin-embedded brains were sectioned and processed for IHC as described in Materials and methods. Bars, 100 μm.

DNA hybridization of brain sections from infected animals. Similar to the findings from the IHC studies described above, only scattered foci of infected cells could be detected (Fig. 2 B). These results demonstrated that MCMV infection of newborn animals resulted in widespread but focal areas of CNS infection.

Mononuclear cells were detected in the meninges of infected mice and in foci containing virus-infected cells, indicating that an inflammatory response within the CNS was associated with this infection (Fig. 3 A). The histological features of these foci included mononuclear cells and in some sections what appeared to be reactive astrogliosis, findings similar to those of microglial nodules that have been described in patients with HCMV encephalitis (3, 22). Both Mac-1$^+$ and Mac-3$^+$ cells

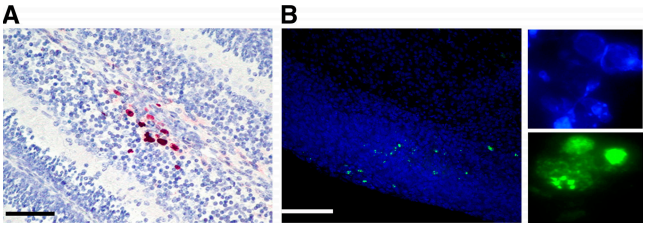

Figure 2. MCMV infection of newborn brain results in focal infection. (A) Section from the cerebellar cortex of a PN day 8–infected mouse was stained with anti-MCMV pp89 mAb to detect virus-infected cells as described in Materials and methods. Focal area of infection is indicated by red staining of nuclei. This section contains a representative focus similar to those seen in sections from >30 animals. Bar, 100 μm. (B) Detection of MCMV DNA by tyramide-amplified in situ hybridization. Frozen sections of brains from infected mice on PN day 8 were hybridized with a tyramide-labeled DNA probe derived from genomic viral DNA and developed as described in Materials and methods. The lower magnification reveals the scattered green foci of infected cells, and the adjacent panels demonstrate at a higher power the signal from the nuclei of infected cells in single foci. Cell nuclei were stained blue with Hoechst dye. Similar results were seen in sections from four mice.

were detected in these infiltrates, suggesting that both resident microglia and peripheral blood monocytes were present in response to virus infection (Fig. 3 A). Activated microglia (F4/80$^+$ and CD45^{intermediate}) and brain macrophages (F4/80$^+$ and CD45^{high}) presumably derived from peripheral blood monocytes were detected by flow cytometric analysis of mononuclear cells from the brains of infected animals (not depicted).

Histological changes were detected as early as 8 d after infection and were temporally correlated with the induction of innate immune responses, including induction of expression of several genes associated with interferon-induced responses (Fig. 3 B). Genes associated with the induction of interferon responses, including IRF-1, IRF-7, USP18, and LRG-47, and class I MHC antigens were shown to be induced by PN day 8 (Fig. 3 B). In addition, the expression of several chemokines was increased in infected animals by PN day 8, including CXCL10, CCL5, and CCL21 (Fig. 3 B). MHC protein expression was present throughout the cerebellar cortex, including areas of the cerebellum without virus infection or infiltration of mononuclear cells. Thus, the induction of gene expression associated with innate immune responses and inflammation in the CNS was not limited to a small number of cells surrounding foci of virus infection but generalized to this entire region of the brain (Fig. 3 C). Finally, there was no evidence of necrosis or significant loss of the resident cellular constituents of the CNS. These results indicated that peripheral infection of newborn mice with MCMV established a generalized but focal encephalitis characterized by infection of resident cells of the brain, accumulation of mononuclear cells, including both resident and infiltrating mononuclear cells, and the induction within entire regions of the brain of inflammatory responses associated with the increased expression of genes associated with innate immune responses.

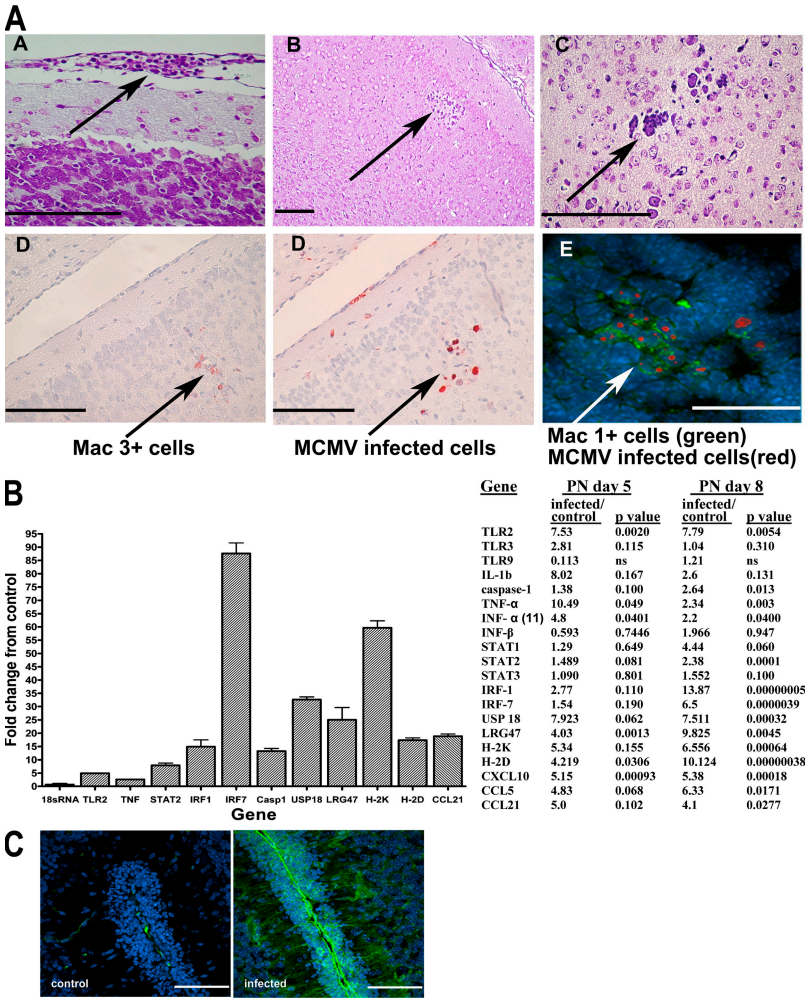

Gene	PN day 5 infected/ control	PN day 5 p value	PN day 8 infected/ control	PN day 8 p value
TLR2	7.53	0.0020	7.79	0.0054
TLR3	2.81	0.115	1.04	0.310
TLR9	0.113	ns	1.21	ns
IL-1b	8.02	0.167	2.6	0.131
caspase-1	1.38	0.100	2.64	0.013
TNF-α	10.49	0.049	2.34	0.003
INF- α (11)	4.8	0.0401	2.2	0.0400
INF-β	0.593	0.7446	1.966	0.947
STAT1	1.29	0.649	4.44	0.060
STAT2	1.489	0.081	2.38	0.0001
STAT3	1.090	0.801	1.552	0.100
IRF-1	2.77	0.110	13.87	0.00000005
IRF-7	1.54	0.190	6.5	0.0000039
USP 18	7.923	0.062	7.511	0.00032
LRG47	4.03	0.0013	9.825	0.0045
H-2K	5.34	0.155	6.556	0.00064
H-2D	4.219	0.0306	10.124	0.00000038
CXCL10	5.15	0.00093	5.38	0.00018
CCL5	4.83	0.068	6.33	0.0171
CCL21	5.0	0.102	4.1	0.0277

Figure 3. MCMV infection of the brain results in mononuclear infiltration and increased expression of innate immune responses. (A) Cellular infiltrates in brains on PN day 10 mice. (A) cellular infiltration of meninges, (B and C) foci of mononuclear cells in the cortex from a PN day 10–infected animal stained with cresyl violet, (D) Mac 3^+ mononuclear cells in the foci of virus-infected cells of a PN day 12 animal by IHC with anti-Mac 3^+ mAb and in an immediately adjacent section (4 μm) of MCMV-infected cells developed with anti-MCMVpp89 as described in Fig. 1, and (E) Mac-1^+ cells in virus-containing foci in a section from a PN day 10–infected animal. Mac-1^+ cells were stained with anti-Mac1 and FITC anti-MIgG (green), and MCMV-infected cells were stained with anti-MCMVpp89 mAb and TRITC anti-MIgG (red). Nuclei were stained with TOPRO III (blue). Bars, 100 μm. (B) Induction of innate immune response in the cerebellum of MCMV-infected mice. Microarray analysis of the expression of selected genes on PN days 5 and 8 RT-PCR was performed as described in Materials and methods. Fold increase in expression in cerebella from infected mice is depicted as the ratio of infected/control mice, and p-value for significant change is shown. Note that in some cases such as IL-1b, eightfold induction was not considered significant ($P > 0.05$ when compared with control animals) based on statistical treatment of array data. Quantitative RT-PCR was used to validate increased expression of interferon-stimulated genes, including USP18, LRG47, and the MHC molecules H-2K and H-2D from nine infected and nine control animals on PN day 8. Fold change in expression between control and infected animals was statistically significant ($P < 0.01$), with the exception of the control 18sRNA template (fold change, 1). (C) Expression of H-2K and H-2D in the saggital section of cerebellum from control and infected mouse PN day 8. Frozen sections were stained with an anti–H-$2K^d$and H-$2D^d$ pan–specific mAb (provided by D. Sachs, Harvard Medical School, Boston, MA) and developed with FITC anti-mIgG, and images were collected using identical settings of laser intensity and detector gain. Note extensive staining of meninges and Bergman glia processes in section from infected animals. Nuclei are stained blue with TOPRO III dye. Bar, 100 μm.

Neonatal MCMV CNS infection results in delayed cerebellar development

Based on the well-described developmental program of the mouse cerebellum in the PN period, we investigated the possibility that infection and inflammation disrupted normal cerebellar architecture. Disruptions of the orderly lamination of the cerebellar cortex could be observed in areas of the cerebellum immediately adjacent to an infectious foci, but such areas of disordered lamination were only rarely associated with virus-infected cells, presumably secondary to the paucity of foci of infection in the brain (not depicted). More striking were global abnormalities in cerebellar cortical development in infected mice that were not spatially associated with adjacent foci of infection or infiltration of inflammatory cells, a finding

reflected by the widespread expression of MHC in the cerebellar cortex (Fig. 3 C). The global dysmorphogenesis was temporally related to the presence of virus in the cerebellum and the induction of genes associated with inflammation (Fig. 3 B). There was a reduction in the foliation of the cerebella from infected animals early after infection (PN days 5–7); however, measurement of the cerebellar area in sagittal sections indicated that the cerebella from infected animals were similar in size to those from control animals until about PN day 9 (Fig. 4, A and B). Cerebella from infected animals were also noted to be smaller than cerebella from control animals on PN days 9–17, and although the cerebella from infected animals remained smaller than cerebella from control animals after PN day 21, this difference was not statistically significant at later time points (Fig. 4 B). The decrease in cerebellar size in infected mice paralleled the kinetics of virus replication in the CNS of infected mice (Fig. 1). Cerebrum weight and volume were similar for both control and MCMV-infected animals on PN days 12, 14, and 17, suggesting that the effect of MCMV infection on CNS development was differentially expressed and limited to regions of the brain developing during the interval of virus infection of the CNS (Fig. 4 B).

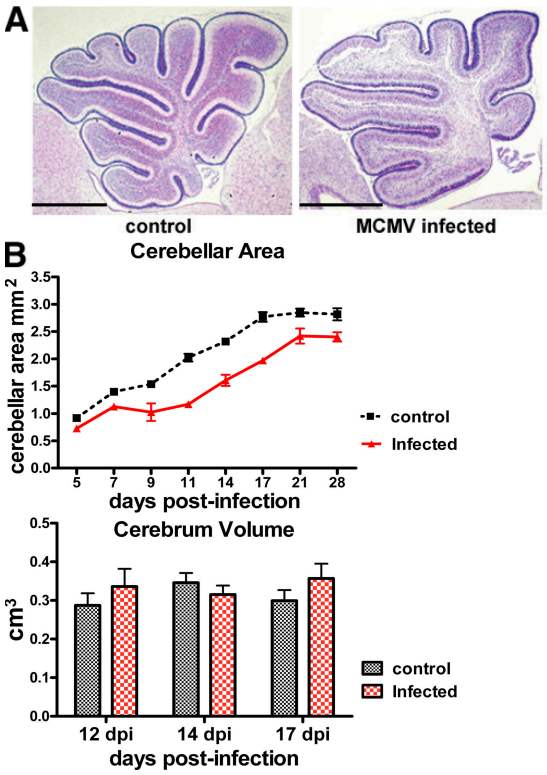

Figure 4. Development of the cerebellum in the PN period is altered by MCMV infection. (A) Cresyl violet staining of the saggital section of cerebellum from a control and MCMV-infected mouse on PN day 7. Note delay in foliation in cerebellum of infected animal. Bars, 1 mm. (B) Cerebellar area from a minimum of five control and MCMV-infected mice at each time point was quantified from a series of 18 saggital sections (4 μm) from each mouse. Mean and standard deviations are indicated by the error bars. The volume of the cerebrum in three to five mice from both infected and control groups was determined at each time point as described in Materials and methods.

A more detailed analysis was performed to characterize the altered morphogenesis of the cerebellum of MCMV-infected mice. Most striking was a persistent and thickened external granular neuron layer (EGL). This difference was apparent at early time points, being most obvious at PN day 7 with a greater than twofold difference in the EGL thickness of infected animals as compared with control animals (Fig. 5 B). The persistence of the EGL in infected animals corresponded with a decrease in the thickness of the internal granular layer (IGL) at later time points, with differences in thickness of the IGL from infected animals and control animals remaining significantly different at PN day 28 (Fig. 5 B). Morphometric analysis also revealed differences in the molecular layer (ML), the acellular layer between the EGL and Purkinje neuron cell body (Fig. 5, A and B). The disparity in the thickness of the ML between infected and control animals was maximal at PN day 14 (infected animals, 70% of controls), a difference that persisted through PN day 28 (Fig. 5 B). The decrease in ML thickness likely reflected a decrease in the number of parallel fiber axons of granular neurons and Purkinje dendrites, major components of this layer. These findings suggested that MCMV infection in newborn mice resulted in a disruption of the normal cellular positioning in the cerebellar cortex.

The morphology of the Purkinje neurons differed between control and infected animals (Fig. 5 A). These abnormalities included diminished arborization of Purkinje dendrites, and less frequently, delayed alignment of the Purkinje neuron cell body leading to ectopia (not depicted). However, the Purkinje neuron cell bodies were similar in size in both infected and control animals (Fig. 5 A). The decrease in Purkinje dendrite arborization was consistent with the observed decrease in thickness of the ML of infected mice (Fig. 5 B). Similar to the changes seen in the EGL, ML, and IGL of the cerebella from infected animals, changes in Purkinje morphology were also global in nature and independent of the presence of an overlying focus of virus infection or inflammation. No obvious morphological changes were noted in the Bergman glia of the cerebellum (not depicted).

Persistence of the EGL in the cerebellar cortex of MCMV-infected mice is associated with delayed granular neuron migration and differentiation

The thickened EGL in the cerebellum of infected animals was inversely related to the area of the cerebellum of infected animals. Thus, we initially explored the possibility that a defect in granule neuron precursor (GNP) cell proliferation and/or migration represented a primary defect after MCMV infection, as these are critical steps in cerebellar cortical development (23, 24). Several possible explanations for the thickened EGL were considered, including an increase in the number of GNPs secondary to (a) decreased apoptosis of GNPs during cerebellar morphogenesis, (b) increased GNP proliferation, and (c) delayed GNP migration.

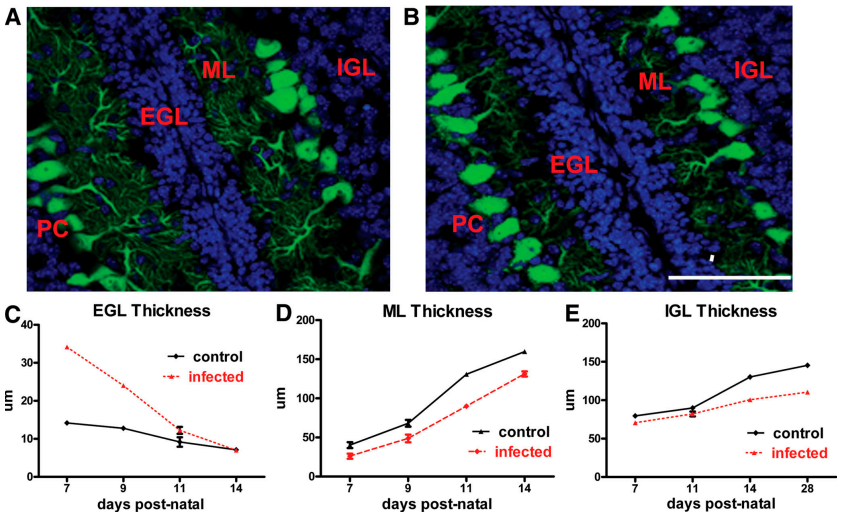

Figure 5. MCMV infection results in the persistence of the EGL and decreased thickness of the IGL and ML in MCMV-infected mice on PN day 10. (A) Immunofluorescent staining of frozen section from representative saggital sections of cerebellum from control and infected mice. Purkinje neurons (PC; green) were stained with calbindin and developed with FITC anti-MIgG. Nuclei were stained with TOPRO III (blue). Note the differences in the thickness of the EGL and ML between sections from the MCMV and control animals. Also note the loss of arborization of the Purkinje dendrites in MCMV-infected as compared with control animals. Bar, 100 μm. (B) Morphometry of the EGL, ML, and IGL was performed on saggital sections, and each data point was derived from six control and infected mice per time point as described in Materials and methods.

We initially examined the possibility that MCMV infection was associated with decreased apoptosis in the developing cerebellum. No differences were found between infected and control animals on PN day 8 when analyzed for activated caspase 3, suggesting that a decrease in GNP apoptosis was an unlikely explanation for the increase in the thickness of the EGL in infected animals (not depicted). We next explored the possibility that the persistence of the EGL in infected mice could be explained by increased proliferation of GNPs in the EGL. GNP proliferation was measured in vivo using BrdU incorporation. After injection of BrdU into mice on PN day 8, BrdU incorporation in cells of the cerebellum was assayed by IHC at 6, 12, and 24 h after injection. More GNPs incorporated BrdU in the control animal group than in the infected group (Fig. 6 A). This result indicated that fewer cells in the EGL of infected animals on PN day 8 were cycling, and that the increased thickness of the EGL in infected mice was not secondary to increased proliferation of GNPs.

The increased cellularity in the EGL of infected animals could be explained by delayed migration of granular neurons from the EGL into deeper layers of the cerebellar cortex. To investigate this possibility, the migration of granular neurons in infected mice was quantified using a modification of the BrdU incorporation assay. Granular neurons of the EGL were pulse-labeled in vivo with BrdU, and brains were harvested at several time points. Consistent with the findings described above, a greater number of cells were labeled with BrdU in the control animal group when compared with infected animals at all time points (Fig. 6, B and C). The proportion of BrdU-labeled neurons that migrated from the EGL was reduced in infected animals compared with control animals. The difference in EGL neuron migration was most striking at 48 h after BrdU inoculation (PN day 10), a time point where significant differences between the thickness of the EGL of infected and control animals were also noted (Fig. 6, B and C). This result suggested that the increased thickness of the EGL in infected animals could be explained by a decreased rate of migration of GNPs from the EGL compared with control animals.

GNP differentiation is delayed in MCMV-infected mice

The findings of decreased GNP proliferation and migration suggested that a defect in GNP differentiation could explain the morphological abnormalities in the cerebella of infected mice. Two molecular markers of granule neuron differentiation state were assayed. TAG-1 (contactin-3) is a secreted glycoprotein selectively expressed by postmitotic granule neurons in the premigratory zone of the EGL (23). In contrast to its distribution in control animals on PN day 8, TAG-1 expression in infected animals was detectable only within the first one to three inner cell layers of the EGL and was not detected in the ML (Fig. 7 A). Cerebellar RNA was then assayed for expression of a developmentally regulated gene, the α 6 subunit of the GABA A receptor (gabra 6). Expression of this receptor has been reported to increase during the first 3 wk of life, making it a useful marker of granule neuron differentiation (25). Expression of gabra 6 was significantly less in the cerebella of infected animals compared with control animals (Fig. 7 B). These results suggested that CNS infection of newborn mice was associated with delayed differentiation of granular neurons.

To more accurately identify the stage of the intrinsic developmental transcriptional program at which GNPs were altered by infection, we assayed the expression of several transcription factors critical for GNP differentiation. These included MATH-1, PAX6, and NeuroD, as these define sequential

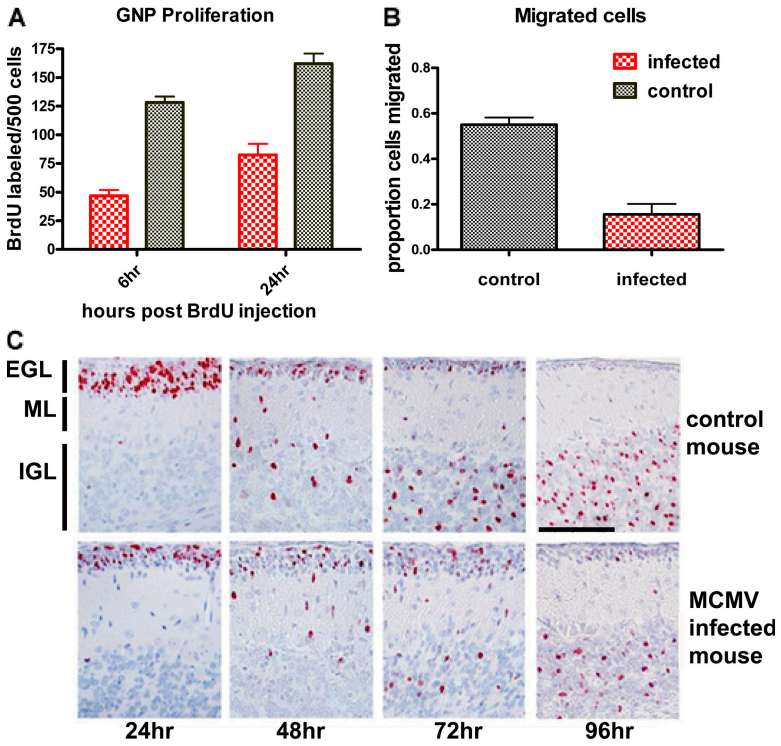

Figure 6. MCMV infection is associated with a decrease in granular neuron proliferation and migration. (A) BrdU incorporation is reduced in the granular neurons of infected mice. Mice were injected with BrdU on PN day 8, and brains were harvested at 6, 12, and 24 h after injection. The number of BrdU staining cells per 500 nucleated cells was determined and plotted as function of time after injection. Only results from 6 and 24 h are shown. Each data point represents findings from six mice. The differences between the groups were significant ($P < 0.002$). (B) Migration of granular neurons is decreased in MCMV-infected animals. MCMV-infected or control animals were injected with BrdU on PN day 8 as described in Materials and methods. Six animals per group were harvested at 24, 48, 72, and 96 h after BrdU injection, and five nonadjacent sagittal sections from the cerebellum were analyzed by IHC using anti-BrdU antibodies. The percentage of migrated cells was calculated by dividing the number of labeled cells in the ML and IGL by the total number of BrdU-expressing cells at 48 h. The differences between the groups were significant ($P < 0.002$). (C) Representative sections from a set of MCMV-infected and control mice. Cells incorporating BrdU are labeled with a red chromogen. Note that differences in migration were most apparent at 48 h after injection, which represents PN day 10 and marginally different at 72 h after injection, findings consistent with morphometry of the EGL (Fig. 5). Bar, 100 µm.

stages of GNP differentiation in the cerebellum (24, 26, 27). The expression of these transcription factors was similar between control and infected animals (not depicted). In addition, no differences were detected in the expression of RNA-encoding sonic hedgehog (Shh) or its receptor, smoothened, in the cerebella of MCMV-infected and control mice (not depicted) (28).

Altered neurotrophin signaling in the cerebellum of MCMV-infected mice

The neurotrophins, nerve growth factor, brain-derived neurotrophic factor (BDNF), and neurotrophin 3 (NT3), were initially suggested to play a major role in the development of the peripheral nervous system by promoting survival of neurons (29). However, these molecules have also been shown to have a role in the development of the CNS (30–34). Two neurotrophins, BDNF and NT3, have been shown to be important in the PN development of the cerebellum (31–34). Genetically engineered mice with a deletion in genes encoding BDNF, Trk B (high affinity BDNF receptor), or Trk C (high affinity NT3 receptor) exhibited altered cerebellar morphogenesis with similarities to the phenotype of MCMV-infected newborn mice (34–37). Initially, we determined the expression of the genes encoding BDNF and its high affinity receptor, Trk B, in both MCMV-infected and control animals on PN days 5 and 8. Similar levels of mRNA were found in both control and MCMV-infected animals when assayed by real-time RT-PCR (not depicted). The expression of mRNA-encoding NT3 and Trk C determined in a microarray analysis were also similar in the cerebella of both control and infected animals (not depicted). Consistent with these results, similar amounts of both the 145-kD full-length Trk B and the 95-kD truncated form of the receptor Trk B were detected in cerebellar lysates from infected and control mice by Western blotting (Fig. 8). However, the expression of activated Trk (phosphorylated tyr^{490}) was estimated to be decreased >10-fold in lysates derived from the cerebella of infected animals as compared with control animals (Fig. 8). Thus, it appeared that MCMV infection was associated with decreased activation of neurotrophin receptors that have been reported previously to play an essential role in cerebellar foliation and lamination, and Purkinje neuron dendrite aborization.

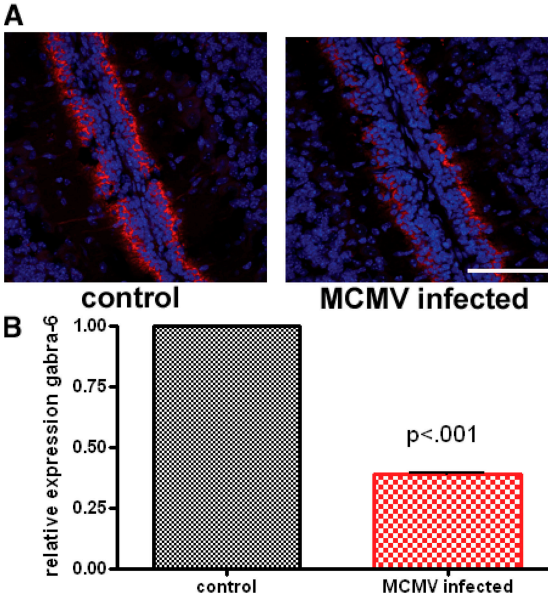

Figure 7. MCMV infection results in delayed expression of neuronal differentiation markers TAG-1 and gabara-6 receptor. (A) Frozen sections from control and MCMV-infected mice on PN day 8 were reacted with anti–TAG-1 mAb followed by TRITC anti-mIgG (red), and nuclei were stained blue with TOPRO III dye. Note the limited extension of TAG-1 staining into the EGL of an infected animal compared with a control animal. Bar, 100 μm. (B) Quantification of gabara-6 mRNA from the cerebellum of control and MCMV-infected mice on PN day 8 by real-time RT-PCR. Values expressed as fold change from controls from four animals per each group. The difference between groups was significant ($P < 0.001$).

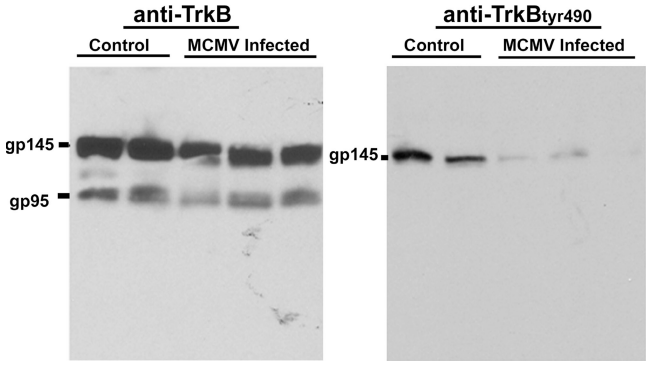

Figure 8. Trk activation is decreased in the cerebellum of MCMV-infected mice. Each sample (lane) analyzed represented pooled cerebella from three mice from control and MCMV-infected mice (total six control and nine MCMV-infected cerebella). The cerebella were lysed and normalized for protein concentration. Equivalent amounts were subjected to SDS-PAGE, transferred to nitrocellulose membranes, and developed with antibodies that were reactive with total Trk B. Antibody binding was detected by ECL. The membrane was stripped and reprobed with antibodies specific for the activated form of Trk (phosphorylated at tyr 490). Note similar levels of Trk B expression but decreased phosphorylated (activated) Trk in cerebella lysates of infected mice.

DISCUSSION

Previous studies have described CNS infection following intracranial inoculation of newborn mice with MCMV (17, 38). These studies reported widespread infection, particularly of cells in the periventricular zones and in those regions of the brain in direct contact with cerebrospinal fluid, similar to descriptions of HCMV ventriculoencephalitis in AIDS patients and infants with severe manifestations of congenital HCMV infection (3, 22). Infection of different resident cells of the CNS and loss of neuroepithelial cells secondary to lytic infection have also been seen in these models (16, 39). In addition, disturbances in granular neuron migration have been reported in organotypic cell cultures infected with MCMV (40). However, descriptions of histopathological findings in human infections, including congenital HCMV infections acquired in utero, suggest that extensive ventricular spread is less frequently seen as compared with hematogenous spread leading to focal areas of parenchymal involvement (3, 6). This latter mechanism of CNS invasion is consistent with the widely scattered foci of infected cells that we observed in the brains of infected mice. Foci-containing virus-infected cells and mononuclear cells closely resembled microglial nodules that have been described in brain sections of autopsy specimens from adult AIDS patients with HCMV encephalitis and fetuses infected in utero with HCMV (3, 22). Because the spread of HCMV to the CNS in patients with AIDS and in congenitally infected infants is believed to be hematogenous, the model of CNS infection described in this report could more accurately reflect key aspects of the pathogenesis of HCMV encephalitis than models that use intracranial virus inoculation. Finally, it is of interest to note that adult mice that were inoculated with MCMV as newborn animals exhibited neurobehavioral deficits manifest by impaired performance on a stationary balance beam, and in preliminary experiments, sensorineural hearing loss was documented in ~15–20% of animals (not depicted). These findings suggest that this model may recapitulate some of the more common neurological sequelae in infants infected with HCMV in utero (4, 5).

The cerebellum is a well-studied region of the rodent brain that undergoes extensive development in the PN period achieving adult architecture between PN days 21 and 28 (24, 25). The population of the EGL by GNPs, their proliferation, and migration into deeper layers of the cerebellar cortex has served as a model system for investigations of cellular positioning in the CNS (23, 25). GNPs migrate tangentially from the primitive rhombic lip of the developing cerebellum and, once positioned in the cerebellar cortex, proliferate in response to several molecular cues (24). Increased cellularity of the EGL and the concomitant increase in cerebellar volume are reflected by an increase in cerebellar size and the characteristic foliation of the cerebellar cortex (24). We observed abnormalities in the cerebella of infected animals that included delays in foliation and the persistence of the EGL in the cerebellar cortex. Cerebellar growth reflected by the cerebellar area was decreased in infected animals between PN days 9 and 18, yet developmental abnormalities such as increased thickness of the EGL and decreased foliation were apparent as early as PN

day 7, a time point at which cerebellar size of control and MCMV-infected mice was indistinguishable. Decreased thickness of the IGL was a second abnormality noted in MCMV-infected animals and presumably resulted from a decrease in granular neuron migration into this layer of the cerebellar cortex. Importantly, cerebellar morphogenesis was altered but not totally arrested by MCMV infection in newborn mice. Finally, the morphological abnormalities in the cerebellar cortex of infected mice were temporally related to virus replication and host inflammatory responses, but were not restricted spatially to areas adjacent to virus-infected cells and mononuclear cell infiltrates. Collectively, these findings suggested that MCMV infection in the CNS of these animals and the associated inflammatory response resulted in a transient interruption or delay in the developmental program of the cerebellum.

A review of the phenotypes of mutant mouse strains suggested several possible defects that could have contributed to the phenotypes of MCMV-infected mice (24, 41–43). Spontaneous mutations in inbred mice leading to loss of Purkinje neurons are associated with decreased proliferation and positioning of granular neurons in the cerebellar cortex (24, 44, 45). Thus, alterations in the granular neuron positioning in infected mice could be secondary to impaired Purkinje neuron function. We did not observe a loss of Purkinje neurons, but this finding did not eliminate the possibility that altered function of these neurons could have potentially contributed to the observed developmental abnormalities.

Several of the morphological abnormalities observed in the cerebella of MCMV-infected mice resemble those described in mutant mice with defects in neurotrophin signaling. The persistence of the EGL in the cerebella of the $BDNF^{-/-}$ transgenic mouse was reminiscent of that seen in MCMV-infected mice (34). $BDNF^{-/-}$ mice have been shown to have thickened EGL, reduced thickness of the ML and IGL, altered Purkinje dendrite arborization, and delayed migration of granular neurons from the EGL to the IGL (34, 46). Interestingly, transgenic mice in which the BDNF receptor Trk B was deleted postnatally exhibited a delay in granular neuron migration, although the phenotype was less striking than the $BDNF^{-/-}$ transgenic mice, possibly reflecting the promiscuity in responses of Trk C receptors to BDNF in these mice (37, 47). Interestingly, morphometry in Trk $B^{-/-}$ transgenic mice performed at ~6 wk of age revealed significant differences in the ML, possibly due to altered development of Purkinje dendrites (47). Abnormalities in cerebellar development have also been described in transgenic mice lacking expression of CAPS2, a protein required for the release of BDNF and NT3 (48). The phenotype of this transgenic mouse included abnormal foliation, persistence of the EGL, and loss of Purkinje dendrite arborization (48). Finally, a spontaneous mutant mouse, *stargazer*, has been shown to have a defect in BDNF expression in the cerebellar granular layer and exhibit delayed migration of granular neurons from the EGL into the IGL (41). Collectively, these findings were consistent for a role of altered neurotrophin expression or signaling in MCMV-infected mice as an explanation for the morphological abnormalities in cerebellar development.

The activities of BDNF are pleiotropic and include protection from neural apoptosis, enhanced neuronal proliferation, increased granular neuron migration, and long-term potentiation (33, 49–51). Recent studies have reported that BDNF can function in an autocrine manner and promote directional migration of granular neurons down a BDNF gradient, a mechanism consistent with a gradient of BDNF production by granular neurons once these cells position themselves in the IGL (52). Activation of the BDNF receptor Trk B in the rodent cerebellum is increased during the first two PN weeks, particularly during the second PN week, and then returns to baseline levels present during embryonic development and adult life, findings that are consistent with the key role of this signaling pathway during cerebellar development (53, 54). Thus, disruption of this signaling pathway during this dynamic time in cerebellar development could result in several abnormalities of morphogenesis, albeit these abnormalities would likely be less pronounced than those observed in $BDNF^{-/-}$ knockout mice, which lack BDNF. Finally, it should also be noted that deletion of the gene encoding of the neurotrophin NT3 resulted in delayed cerebellar foliation, a phenotype that was similar to that of newborn mice infected with MCMV (35). The analysis of the cerebella of $NT3^{-/-}$ mice did not reveal abnormalities in GNP proliferation or migration, but an increased frequency of apoptotic cells in the cerebellum (35).

Our findings indicated that the phosphorylation of tyr 490 on Trk receptors was significantly decreased in the cerebella of infected animals compared with control animals. The availability of antibodies specific for individual phosphorylated Trks is limited, and the commonly used antibody against the tyr 490 is reactive with all phosphorylated Trks (Trk A, B, and C); therefore, it was not possible to determine which specific Trk was phosphorylated in cerebellar lysates analyzed in this study. We failed to detect Trk A in the cerebellar lysates from infected and control animals using a Trk A–specific antibody, suggesting that the decrease in phosphorylated Trks was not secondary to the decrease in phosphorylated Trk A (unpublished data), a result consistent with previous studies demonstrating that Trk A was not activated in the cerebella of newborn mice (53, 55). Although we could not definitely determine if Trk B, Trk C, or both were hypophosphorylated with available antibodies, our results do argue for a potentially biologically important effect associated with decreased activation of Trk B and/or Trk C in MCMV-infected mice. Lastly, the assignment of a key function exclusively to either Trk B or Trk C signaling could be arbitrary because of documented promiscuity in receptor activation by BDNF and NT3 (29, 37, 56, 57). The pathways through which virus infection and/or inflammation in the developing CNS alter Trk B (and/or Trk C) activation in the cerebellum of infected animals are unknown but could be secondary to disruption of transcriptional or posttranslational regulation, including the relocalization of this receptor to the cell surface (58–60).

The mechanism(s) responsible for delayed cerebellar development and cellular positioning in MCMV-infected mice remains undefined. Virus infection of the CNS in these animals

is focal, and widespread necrosis and loss of cellular populations in infected brains cannot be appreciated. Thus, it is likely that soluble mediators associated with the inflammatory response contributed to the global changes seen in the developing cerebellum. CNS disease linked to inflammatory responses of resident cells of the CNS after infection of newborn mice with nonlytic viruses such as murine leukemia virus (MuLV) or Borna disease virus (BDV) has been described (61–63). MuLV infection of newborn mice results in neurological disease associated with minimal neuropathology (64). The CNS disease in MuLV-infected animals appears to be mediated through activated glial cells and release of inflammatory molecules (63). Inoculation of newborn rats with BDV has been shown to cause altered cerebellar morphology and decreased cerebellar area in the absence of widespread cell lysis (61, 65). The tropism of BDV for Purkinje neurons has been suggested as an explanation of the generalized alterations in cereballar development seen in BDV-infected animals (66, 67). Subsequent studies in this system have described inflammatory responses of astroglial and microglial cells and the release of soluble mediators of inflammation, including cytokines, which may also contribute to the neuropathology in BDV-infected animals (61, 68, 69). Finally, transgenic mice expressing interferon-γ under control of a myelin basic promoter or transgenic mice overexpressing TNF-α also exhibited delayed migration from the EGL, findings consistent with the role of inflammatory mediators in the altered cerebellar development in MCMV-infected mice (70, 71). Our results demonstrated foci of mononuclear cells early after virus infection of the brain along with expression of the proinflammatory cytokine TNF-α and the increased expression of components of the innate response, such as TLR-2, interferon-α, IRF-1, IRF-7, and Stat-2, as well as several interferon-stimulated genes. Thus, we believe that inflammatory response generated early in MCMV infection of the brain and the production of soluble mediators of inflammation could either directly or indirectly alter the developmental program of the cerebellum.

We have not identified specific proinflammatory molecules responsible for the altered developmental programs of cells of the cerebellum, but chemokines are known to play a role in cellular positioning during cerebellar development (72, 73). In MCMV-infected animals, up-regulation of chemokine gene expression in the cerebellum was detected early in infection, raising the possibility that these soluble molecules could affect GNP differentiation and positioning. The precise mechanism(s) through which inflammatory mediators alter cerebellar development and Trk activation is unknown, but possible mechanisms include chemokine coupling of GPCR with $G_{\alpha I}$, inhibition of adenylyl cyclase, and cAMP production with subsequent decreased activation of PKA (74). Inhibition of cAMP production and PKA activation has been shown to inhibit Purkinje dendrite morphogenesis through reduced activation of Trk B (49). Thus, a decrease in cAMP production by inhibition of adenylyl cyclase and/or increased protein phosphatase 1 activity could result in decreased activation of Trk B after exposure of cells to limiting concentrations of BDNF (75, 76). Reports describing cAMP-controlled recruitment of intracellular Trk B to the plasma membrane are also consistent with this mechanism (58–60). Thus, the tightly regulated activation of this key neurotrophin receptor in the cerebellum could potentially be altered by soluble mediators of the inflammation associated with the response to MCMV infection.

MATERIALS AND METHODS

Mice, virus infections, and virus titration

Newborn (<24-h-old) BALB/c mice were inoculated intraperitoneally with 200 PFU of tissue culture–derived Smith strain of MCMV (Smith strain, VR-194 [recently reaccessioned as VR-1399]; American Type Culture Collection [ATCC]). In the initial experiments in which virus replication and cerebellar morphometry were performed, animals were given equivalent amounts of media and designated as mock infected. Subsequently, we used noninfected animals as controls, as we could not detect differences in terms of cerebellar morphology or histology between media-inoculated (mock-infected) or noninfected animals. Mice were harvested at various PN days after they were killed. The animals were perfused extensively with PBS by insertion of plastic canula into the left ventricle and transection of the inferior vena cava. The organs were weighed, and a 10% wt/vol homogenate in media and viral titers in the brain and liver were determined by standard plaque assay on mouse embryonic fibroblast (77). The limit of detection was estimated at 10^2 infectious U/g of tissue. Results are expressed as PFU/g of tissue. Pathogen-free male and female BALB/c mice were purchased from Charles River Laboratories for experiments performed at the University of Alabama at Birmingham. All breeding and experiments were performed in accordance with the guidelines of the University of Alabama at Birmingham, University Institutional Animal Care and Use Committee, and with animal use policies monitored by the Animal Use Committee at the University of Rijeka. All animal use protocols and animal care procedures at the University of Rijeka were also reviewed by the University Institutional Animal Care and Use Committee at the University of Alabama at Birmingham.

Cerebellar morphometry

For morphometry, mice were killed on PN days 5–28 and perfused with PBS, pH 7.4, followed by perfusion with 4% PFA in PBS. After fixation, the brains were divided in two parts at the midline and embedded in paraffin. 4-μm sagittal serial sections were processed for further analysis, and ~18 slides per brain were studied. Results shown are average value for each animal for the group of five to six animals per time point. Morphometric measurements of cerebellar area and circumference were performed on cresyl violet-stained sections using ImagePro software (MediaCybernetics). Cerebral volumes of infected and uninfected animals were measured by use of a water-displacement method (78). The thickness of the EGL and other layers of the cerebellar cortex were measured on the same sections at six points along the primary fissure and expressed as the average of all measurements for each animal.

Histology, immunohistochemistry, and immunofluorescence assays

After fixation, the brains from infected and noninfected animals were divided in two parts at midline and embedded in paraffin for sectioning. 4-μm sagittal sections were cut from the midline of the cerebellum and processed for cresyl violet histological staining and/or immunohistochemistry. IHC staining for the IE protein (pp89) encoded by MCMV IE-1 was performed as described previously (21). IHC staining of Purkinje, astroglia, and microglial cells was performed using anti–calbindin D28 (Sigma-Aldrich), anti-GFAP, anti–mouse Mac-3 (BD Biosciences), or anti-BrdU (Sigma-Aldrich) as primary antibodies, respectively. For BrdU detection, slides were incubated in 2N HCl before antibody detection. The antibody binding was visualized with biotinylated goat anti–mouse Ig and mouse anti–rat IgG1/2a (BD Biosciences), followed by streptavidin peroxidase and 3, 3′-diaminobenzidine (black staining) or 3- amino-9-ethylcarbazole (red staining; Sigma-Aldrich) as chromogens. Sections were counterstained with hematoxylin.

For immunofluorescence images, animals were killed and perfused with 4% paraformaldehyde (PFA) as described above. The brains were soaked in cold PFA for ~4 h, followed by three 4-h PBS washes to remove PFA from tissue, and then soaked until they sunk to the bottom of the container in 30% sucrose as a cryoprotectant during the freezing. Brains were then split midsaggitally, embedded in Tissue Tek freezing media, and frozen on dry ice. Sections were cut on a Leica cryostat at 8-μM thickness. Sections were probed with primary antibody and fluorescent secondary antibodies. Primary antibodies used were calbindin D28 (Sigma-Aldrich), Tag-1/4D7, Mac-1 (Developmental Studies Hybridoma Bank, University of Iowa, Iowa City, Iowa), MCMV IE1 (see above), anti–H-2K^d, H-2D^d, H-2L^d mAb 34–1-2S (ATCC) and cleaved caspase 3 (Cell Signaling Technology). For cleaved caspase 3 detection, positive controls consisted of the brains from PN days 5–8 mice given ethanol 8–12 h before harvesting. Antibody binding was detected with an Olympus laser confocal microscope.

In situ hybridization

Bacterial artificial chromosomes containing the MCMV genome were nick translated and biotin labeled with an Invitrogen Bionick biotin probe labeling kit. The reaction was stopped after 2 h when the probe size was roughly 500 bp in length. Details of the tissue treatment have been described (79). After overnight hybridization, streptavidin horseradish peroxidase–conjugated antibodies were applied, and tyramide amplification with fluorophore deposition was used to detect viral nucleic acids (79).

Proliferation and migration assays

Proliferation assay. MCMV-infected or control newborn mice were injected intraperitoneally with BrdU (50 μg/g body weight) 8 d after infection. Mice were killed 6, 12, and 24 h after BrdU administration and perfused with 4% PFA before paraffin embedding. Incorporation of BrdU was assessed in five nonadjacent sagittal sections on folia VI within the primary fissure. For analysis of proliferation, the number of BrdU-labeled nuclei per 500 nucleated cells was determined in external granular layer.

Migration assay. For migration assay, the MCMV-infected or control newborn mice were injected with BrdU as described above on PN day 8. Mice were killed 24, 48, 72, and 96 h after BrdU administration and perfused with 4% PFA before paraffin embedding. For analysis of granular cell migration, the number of BrdU-labeled cells/mm in each cortical layer was counted in five nonadjacent sagittal sections of folia VI within primary fissure. Duodenum was taken for control of BrdU incorporation.

Microarray analysis of cerebellar RNA by quantitative PCR

Target labeling and hybridization for mouse exonic evidence base oligonucleotide–spotted array. Cerebellar RNA was isolated from neonatal-infected and control-noninfected mice on PN days 5, 8, and 12 using Trizol reagent (Roche) and rotor homogenization. Isolation of RNA and elimination of DNA contamination were performed with QIAGEN RNEASY columns with QIAGEN DNASe. All RNA Preps submitted to the Vanderbilt Medical School Shared Array Resource (http://array.mc.vanderbilt.edu/) were run on an Agilent 2100 Bioanalyzer to assess RNA integrity. Those samples meeting minimum requirements of RI*n* value of 7.0 and greater were used to generate cDNA targets for hybridization to spotted arrays in the following manner: 5–10 μg of total RNA from each sample was reverse transcribed at 42°C using 400 U Superscript II (Invitrogen) in the presence of 6 μg of anchored oligo dT and an amino-allyl–tagged dUTP (Sigma-Aldrich). Additionally, RNA spike-in controls (Ambion) were added at concentrations ranging from 0 to 200 pg per spike per reverse-transcription reaction. These eight control spike-ins hybridize to the Ambion control spots on VMSR arrays. Final concentrations of dNTPs in the reaction were 200uM dA,dG,dC, 51uM dT, and 149uM AAdUTP (Sigma-Aldrich). cDNA targets generated were incubated with NaOH to hydrolyze any remaining total RNA, and then neutralized with HCl and purified over Qiaquick PCR purification columns (QIAGEN) according to the manufacturer's protocol, with the following exception: two washes were completed with 80% ETOH instead of PE buffer, and the elution was completed with nuclease-free H_2O instead of EB buffer. The targets were dried to completion and coupled to either ester-linked Cy5 or Cy3 dyes (GE Healthcare) in 0.1 M sodium bicarbonate, pH. 9.0, for 60 min in a 6-μl volume to facilitate the coupling reaction. After quenching of unbound dye with 4 M hydroxylamine (Sigma-Aldrich), Cy3 and Cy5 pairs were combined and the target pairs were again purified over Qiaquick columns (QIAGEN) and dried to completion in a speed-vac. The targets were then resuspended in 50 μl of MWG Hyb Buffer (Ocimum Biosolutions), and 1 μg poly A RNA (Sigma-Aldrich) was added to each target. The targets were heat denatured and then hybridized for 16 h at 42°C on a Maui Hyb Station (BioMicro Systems). Mouse exonic evidence base oligonucleotide arrays were used for these array analyses (MEEBO; http://www.microarray.org./sfgf/meebo.do). After hybridization washes, all arrays were scanned on an AXON 4,000b scanner.

Microarray data analysis

Microarray gene pix scan results were loaded into statistical software, HDBSTAT (www.soph.uab.edu/ssg/default.aspx?id=91). Quantile–quantile normalization was performed to maximize statistical power by converting raw expression levels into ranks. After normalization, Welch or Student's *t* test was performed comparing control to infected samples. Data were output in Excel file format and sorted by p-value. The original raw data were also examined with commercial GeneTraffic software after Lowess subgrid normalization. The data from this microarray analysis has been deposited in the GEO database under accession number GSE9945.

Quantitative RT-PCR

After RNA isolation, Invitrogen first-strand synthesis with retrovirus-derived reverse transcription and random hexamers was performed. Gene-specific primers were designed with Primer Express software (Applied Biosystems). SYBR green real-time quantitative PCR was used to amplify genes from the reverse-transcribed cerebellar RNA. 18S ribosomal subunit primers were used to normalize cDNA loading amounts (80). Gel electrophoresis and melt curves were used to confirm amplicon identity. For primer design, coding sequence was blasted against the mouse sequence database of National Center for Biotechnology Information to determine unique sequence regions for primer selection, which was then input to PrimerExpress software from ABI. Six pooled samples with four mouse cerebella per pool were used for each PCR. 1 μl of this RT reaction was serially diluted 10-fold five times. The first dilution was used as template for gene-specific priming, and the three terminal dilutions were used for 18S loading controls. The ratio of cycle threshold (Ct) for 18S was used to correct loading errors. The corrected values were then used to calculate three separate Ct differences, and these differences were then used to compute the average Ct difference and column statistics.

Western immunoblotting

Western blotting using standard 10% acrylamide gels and denaturing conditions was used to detect Trk B and phosphorylated Trks. Cerebellar tissue from control and infected mice on PN days 5 and 8 were rapidly homogenized on ice in RIPA buffer with dounce homogenizers. After low speed centrifugation to remove large debris, lysates were mixed with SDS loading buffer (5% 2-mercaptoethanol, 2% SDS, tris, pH 8.8) and boiled, spun, and loaded onto acrylamide gels for electrophoresis. Protein loading was equalized by quantitation of total protein using a Thermo Fisher Scientific BCA protein assay kit with albumin standards. Protein was transferred to nitrocellulose membrane and blocked and probed with primary antibody. After development with anti–Trk B antibodies, the membranes were stripped with Restore Stripping Reagent (Thermo Fisher Scientific) and reprobed with anti-p490 Trk A/B antibodies. Antibodies used were Trk B (BD Transduction Laboratories) and p490 Trk A/B (Cell Signaling Technology). Secondary horseradish peroxidase–conjugated antibody detection was performed with chemiluminescence reagents (Supersignal West Picomole; Thermo Fisher Scientific) and film development.

The authors would like to thank Dr. Grier Page (School of Public Health, UAB, Birmingham, AL) for help with analysis and presentation of microarray data.

This work was supported by a grant from the National Institutes of Health (NIH), National Institute of Child Health and Human Development (R01 HD044721;

to W.J. Britt) and support from the Croatian Ministry of Science and Technology (to S. Jonjic). T. Koontz was supported by the NIH training grant 5 T32 AI007150-30.

The authors have no conflicting financial interests.

Submitted: 19 July 2007
Accepted: 8 January 2008

REFERENCES

1. Gonzalez-Scarano, F., and J. Martin-Garcia. 2005. The neuropathogenesis of AIDS. *Nat. Rev. Immunol.* 5:69–81.
2. Kaul, M., and S.A. Lipton. 2006. Mechanisms of neuronal injury and death in HIV-1 associated dementia. *Curr. HIV Res.* 4:307–318.
3. Becroft, D.M.O. 1981. Prenatal cytomegalovirus infection: epidemiology, pathology, and pathogenesis. *In* Perspective in Pediatric Pathology. H.S. Rosenberg and J. Bernstein, editors. Masson Press, New York. 203–241.
4. Fowler, K.B., S. Stagno, R.F. Pass, W.J. Britt, T.J. Boll, and C.A. Alford. 1992. The outcome of congenital cytomegalovirus infection in relation to maternal antibody status. *N. Engl. J. Med.* 326:663–667.
5. Stagno, S., and W.J. Britt. 2006. Cytomegalovirus. *In* Infectious Diseases of the Fetus and Newborn Infant, 6th Edition. J.S. Remington and J.O. Klein, editors. W.B. Saunders, Philadelphia. 203–241.
6. Perlman, J.M., and C. Argyle. 1992. Lethal cytomegalovirus infection in preterm infants: clinical, radiological, and neuropathological findings. *Ann. Neurol.* 31:64–68.
7. Dahle, A.J., K.B. Fowler, J.D. Wright, S.B. Boppana, W.J. Britt, and R.F. Pass. 2000. Longitudinal investigation of hearing disorders in children with congenital cytomegalovirus. *J. Am. Acad. Audiol.* 11:283–290.
8. de Vries, L.S., H. Gunardi, P.G. Barth, L.A. Bok, M.A. Verboon-Maciolek, and F. Groenendaal. 2004. The spectrum of cranial ultrasound and magnetic resonance imaging abnormalities in congenital cytomegalovirus infection. *Neuropediatrics.* 35:113–119.
9. Barkovich, A.J., and C.E. Lindan. 1994. Congenital cytomegalovirus infection of the brain: imaging analysis and embryologic considerations. *AJNR Am. J. Neuroradiol.* 15:703–715.
10. Becroft, D.M. 1981. Prenatal cytomegalovirus infection: epidemiology, pathology and pathogenesis. *Perspect. Pediatr. Pathol.* 6:203–241.
11. Marques Dias, M.J., G. Harmant-van Rijckevorsel, P. Landrieu, and G. Lyon. 1984. Prenatal cytomegalovirus disease and cerebral microgyria: evidence for perfusion failure, not disturbance of histogenesis, as the major cause of fetal cytomegalovirus encephalopathy. *Neuropediatrics.* 15:18–24.
12. Pizzorno, M.C., M.A. Mullen, Y.N. Chang, and G.S. Hayward. 1991. The functionally active IE2 immediate-early regulatory protein of human cytomegalovirus is an 80-kilodalton polypeptide that contains two distinct activator domains and a duplicated nuclear localization signal. *J. Virol.* 65:3839–3852.
13. Boesch, C., J. Issakainen, G. Kewitz, R. Kikinis, E. Martin, and E. Boltshauser. 1989. Magnetic resonance imaging of the brain in congenital cytomegalovirus infection. *Pediatr. Radiol.* 19:91–93.
14. Griffith, B.P., and M.J. Aquino-de Jesus. 1991. Guinea pig model of congenital cytomegalovirus infection. *Transplant. Proc.* 23:29–31.
15. Woolf, N.K., F.J. Koehrn, J.P. Harris, and D.D. Richman. 1989. Congenital cytomegalovirus labyrinthitis and sensorineural hearing loss in guinea pigs. *J. Infect. Dis.* 160:929–937.
16. Kosugi, I., Y. Shinmura, H. Kawasaki, Y. Arai, R.Y. Li, S. Baba, and Y. Tsutsui. 2000. Cytomegalovirus infection of the central nervous system stem cells from mouse embryo: a model for developmental brain disorders induced by cytomegalovirus. *Lab. Invest.* 80:1373–1383.
17. van den Pol, A.N., J.D. Reuter, and J.G. Santarelli. 2002. Enhanced cytomegalovirus infection of developing brain independent of the adaptive immune system. *J. Virol.* 76:8842–8854.
18. Tarantal, A.F., M.S. Salamat, W.J. Britt, P.A. Luciw, A.G. Hendrickx, and P.A. Barry. 1998. Neuropathogenesis induced by rhesus cytomegalovirus in fetal rhesus monkeys (Macaca mulatta). *J. Infect. Dis.* 177:446–450.
19. Chang, W.L., A.F. Tarantal, S.S. Zhou, A.D. Borowsky, and P.A. Barry. 2002. A recombinant rhesus cytomegalovirus expressing enhanced green fluorescent protein retains the wild-type phenotype and pathogenicity in fetal macaques. *J. Virol.* 76:9493–9504.
20. Bradford, R., G. Bantug, T. Koontz, M. Golemac, S. Jonjic, and W. Britt. 2007. Possible role of cell-free virus in dissemination of CMV to the developing CNS. *In* 11th International CMV and Betaherpesvirus Workshop. Toulouse, France. 151.
21. Trgovcich, J., D. Stimac, B. Polic, A. Krmpotic, E. Pernjak-Pugel, J. Tomac, M. Hasan, B. Wraber, and S. Jonjic. 2000. Immune responses and cytokine induction in the development of severe hepatitis during acute infections with murine cytomegalovirus. *Arch. Virol.* 145:2601–2618.
22. Arribas, J.R., G.A. Storch, D.B. Clifford, and A.C. Tselis. 1996. Cytomegalovirus encephalitis. *Ann. Intern. Med.* 125:577–587.
23. Hatten, M.E. 1999. Central nervous system neuronal migration. *Annu. Rev. Neurosci.* 22:511–539.
24. Goldowitz, D., and K. Hamre. 1998. The cells and molecules that make a cerebellum. *Trends Neurosci.* 21:375–382.
25. Kuhar, S.G., L. Feng, S. Vidan, M.E. Ross, M.E. Hatten, and N. Heintz. 1993. Changing patterns of gene expression define four stages of cerebellar granule neuron differentiation. *Development.* 117:97–104.
26. Schuller, U., A.T. Kho, Q. Zhao, Q. Ma, and D.H. Rowitch. 2006. Cerebellar 'transcriptome' reveals cell-type and stage-specific expression during postnatal development and tumorigenesis. *Mol. Cell. Neurosci.* 33:247–259.
27. Morales, D., and M.E. Hatten. 2006. Molecular markers of neuronal progenitors in the embryonic cerebellar anlage. *J. Neurosci.* 26:12226–12236.
28. Wechsler-Reya, R.J., and M.P. Scott. 1999. Control of neuronal precursor proliferation in the cerebellum by Sonic Hedgehog. *Neuron.* 22:103–114.
29. Huang, E.J., G.A. Wilkinson, I. Farinas, C. Backus, K. Zang, S.L. Wong, and L.F. Reichardt. 1999. Expression of Trk receptors in the developing mouse trigeminal ganglion: in vivo evidence for NT-3 activation of TrkA and TrkB in addition to TrkC. *Development.* 126:2191–2203.
30. Rocamora, N., F.J. Garcia-Ladona, J.M. Palacios, and G. Mengod. 1993. Differential expression of brain-derived neurotrophic factor, neurotrophin-3, and low-affinity nerve growth factor receptor during the postnatal development of the rat cerebellar system. *Brain Res. Mol. Brain Res.* 17:1–8.
31. Schwartz, P.M., R.L. Levy, P.R. Borghesani, and R.A. Segal. 1998. Cerebellar pathology in BDNF−/− mice: the classic view of neurotrophins is changing. *Mol. Psychiatry.* 3:116–120.
32. Borghesani, P.R., J.M. Peyrin, R. Klein, J. Rubin, A.R. Carter, P.M. Schwartz, A. Luster, G. Corfas, and R.A. Segal. 2002. BDNF stimulates migration of cerebellar granule cells. *Development.* 129:1435–1442.
33. Carter, A.R., C. Chen, P.M. Schwartz, and R.A. Segal. 2002. Brain-derived neurotrophic factor modulates cerebellar plasticity and synaptic ultrastructure. *J. Neurosci.* 22:1316–1327.
34. Schwartz, P.M., P.R. Borghesani, R.L. Levy, S.L. Pomeroy, and R.A. Segal. 1997. Abnormal cerebellar development and foliation in BDNF−/− mice reveals a role for neurotrophins in CNS patterning. *Neuron.* 19:269–281.
35. Bates, B., M. Rios, A. Trumpp, C. Chen, G. Fan, J.M. Bishop, and R. Jaenisch. 1999. Neurotrophin-3 is required for proper cerebellar development. *Nat. Neurosci.* 2:115–117.
36. Li, S., F. Qiu, A. Xu, S.M. Price, and M. Xiang. 2004. Barhl1 regulates migration and survival of cerebellar granule cells by controlling expression of the neurotrophin-3 gene. *J. Neurosci.* 24:3104–3114.
37. Minichiello, L., and R. Klein. 1996. TrkB and TrkC neurotrophin receptors cooperate in promoting survival of hippocampal and cerebellar granule neurons. *Genes Dev.* 10:2849–2858.
38. Shinmura, Y., I. Kosugi, S. Aiba-Masago, S. Baba, L.R. Yong, and Y. Tsutsui. 1997. Disordered migration and loss of virus-infected neuronal cells in developing mouse brains infected with murine cytomegalovirus. *Acta Neuropathol.* 93:551–557.
39. van Den Pol, A.N., E. Mocarski, N. Saederup, J. Vieira, and T.J. Meier. 1999. Cytomegalovirus cell tropism, replication, and gene transfer in brain. *J. Neurosci.* 19:10948–10965.
40. Shinmura, Y., I. Kosugi, M. Kaneta, and Y. Tsutsui. 1999. Migration of virus-infected neuronal cells in cerebral slice cultures of developing mouse brains after in vitro infection with murine cytomegalovirus. *Acta Neuropathol.* 98:590–596.

41. Qiao, X., L. Chen, H. Gao, S. Bao, F. Hefti, R.F. Thompson, and B. Knusel. 1998. Cerebellar brain-derived neurotrophic factor-TrkB defect associated with impairment of eyeblink conditioning in Stargazer mutant mice. *J. Neurosci.* 18:6990–6999.
42. Jensen, P., R. Smeyne, and D. Goldowitz. 2004. Analysis of cerebellar development in math1 null embryos and chimeras. *J. Neurosci.* 24:2202–2211.
43. Mullen, R.J., K.M. Hamre, and D. Goldowitz. 1997. Cerebellar mutant mice and chimeras revisited. *Perspect. Dev. Neurobiol.* 5:43–55.
44. Smeyne, R.J., T. Chu, A. Lewin, F. Bian, S. Sanlioqlu, C. Kunsch, S.A. Lira, and J. Oberdick. 1995. Local control of granule cell generation by cerebellar Purkinje cells. *Mol. Cell. Neurosci.* 6:230–251.
45. Baptista, C.A., M.E. Hatten, R. Blazeski, and C.A. Mason. 1994. Cell-cell interactions influence survival and differentiation of purified Purkinje cells in vitro. *Neuron.* 12:243–260.
46. Jones, K.R., I. Farinas, C. Backus, and L.F. Reichardt. 1994. Targeted disruption of the BDNF gene perturbs brain and sensory neuron development but not motor neuron development. *Cell.* 76:989–999.
47. Rico, B., B. Xu, and L.F. Reichardt. 2002. TrkB receptor signaling is required for establishment of GABAergic synapses in the cerebellum. *Nat. Neurosci.* 5:225–233.
48. Sadakata, T., W. Kakegawa, A. Mizoguchi, M. Washida, R. Katoh-Semba, F. Shutoh, T. Okamoto, H. Nakashima, K. Kimura, M. Tanaka, et al. 2007. Impaired cerebellar development and function in mice lacking CAPS2, a protein involved in neurotrophin release. *J. Neurosci.* 27:2472–2482.
49. Ji, Y., P.T. Pang, L. Feng, and B. Lu. 2005. Cyclic AMP controls BDNF-induced TrkB phosphorylation and dendritic spine formation in mature hippocampal neurons. *Nat. Neurosci.* 8:164–172.
50. Shimada, A., C.A. Mason, and M.E. Morrison. 1998. TrkB signaling modulates spine density and morphology independent of dendrite structure in cultured neonatal Purkinje cells. *J. Neurosci.* 18:8559–8570.
51. Barco, A., S. Patterson, J.M. Alarcon, P. Gromova, M. Mata-Roig, A. Morozov, and E.R. Kandel. 2005. Gene expression profiling of facilitated L-LTP in VP16-CREB mice reveals that BDNF is critical for the maintenance of LTP and its synaptic capture. *Neuron.* 48:123–137.
52. Zhou, P., M. Porcionatto, M. Pilapil, Y. Chen, Y. Choi, K.F. Tolias, J.B. Bikoff, E.J. Hong, M.E. Greenberg, and R.A. Segal. 2007. Polarized signaling endosomes coordinate BDNF-induced chemotaxis of cerebellar precursors. *Neuron.* 55:53–68.
53. Knusel, B., S.J. Rabin, F. Hefti, and D.R. Kaplan. 1994. Regulated neurotrophin receptor responsiveness during neuronal migrationand early differentiation. *J. Neurosci.* 14:1542–1554.
54. Gao, W.Q., J.L. Zheng, and M. Karihaloo. 1995. Neurotrophin-4/5 (NT-4/5) and brain-derived neurotrophic factor (BDNF) act at later stages of cerebellar granule cell differentiation. *J. Neurosci.* 15:2656–2667.
55. Gao, Y., E. Nikulina, W. Mellado, and M.T. Filbin. 2003. Neurotrophins elevate cAMP to reach a threshold required to overcome inhibition by MAG through extracellular signal-regulated kinase-dependent inhibition of phosphodiesterase. *J. Neurosci.* 23:11770–11777.
56. Segal, R.A. 2003. Selectivity in neurotrophin signaling: theme and variations. *Annu. Rev. Neurosci.* 26:299–330.
57. Doughty, M.L., A. Lohof, A. Campana, N. Delhaye-Bouchaud, and J. Mariani. 1998. Neurotrophin-3 promotes cerebellar granule cell exit from the EGL. *Eur. J. Neurosci.* 10:3007–3011.
58. Meyer-Franke, A., G.A. Wilkinson, A. Kruttgen, M. Hu, E. Munro, M.G. Hanson Jr., L.F. Reichardt, and B.A. Barres. 1998. Depolarization and cAMP elevation rapidly recruit TrkB to the plasma membrane of CNS neurons. *Neuron.* 21:681–693.
59. Deogracias, R., G. Espliguero, T. Iglesias, and A. Rodriguez-Pena. 2004. Expression of the neurotrophin receptor trkB is regulated by the cAMP/CREB pathway in neurons. *Mol. Cell. Neurosci.* 26:470–480.
60. Nagappan, G., and B. Lu. 2005. Activity-dependent modulation of the BDNF receptor TrkB: mechanisms and implications. *Trends Neurosci.* 28:464–471.
61. Jordan, I., and W.I. Lipkin. 2001. Borna disease virus. *Rev. Med. Virol.* 11:37–57.
62. Peterson, K.E., S.J. Robertson, J.L. Portis, and B. Chesebro. 2001. Differences in cytokine and chemokine responses during neurological disease induced by polytropic murine retroviruses Map to separate regions of the viral envelope gene. *J. Virol.* 75:2848–2856.
63. Peterson, K.E., J.S. Errett, T. Wei, D.E. Dimcheff, R. Ransohoff, W.A. Kuziel, L. Evans, and B. Chesebro. 2004. MCP-1 and CCR2 contribute to non-lymphocyte-mediated brain disease induced by Fr98 polytropic retrovirus infection in mice: role for astrocytes in retroviral neuropathogenesis. *J. Virol.* 78:6449–6458.
64. Portis, J.L., S. Czub, S. Robertson, F. McAtee, and B. Chesebro. 1995. Characterization of a neurologic disease induced by a polytropic murine retrovirus: evidence for differential targeting of ecotropic and polytropic viruses in the brain. *J. Virol.* 69:8070–8075.
65. Zocher, M., S. Czub, J. Schulte-Monting, J.C. de La Torre, and C. Sauder. 2000. Alterations in neurotrophin and neurotrophin receptor gene expression patterns in the rat central nervous system following perinatal Borna disease virus infection. *J. Neurovirol.* 6:462–477.
66. Williams, B.L., K. Yaddanapudi, M. Hornig, and W.I. Lipkin. 2007. Spatiotemporal analysis of purkinje cell degeneration relative to parasagittal expression domains in a model of neonatal viral infection. *J. Virol.* 81:2675–2687.
67. Eisenman, L.M., R. Brothers, M.H. Tran, R.B. Kean, G.M. Dickson, B. Dietzschold, and D.C. Hooper. 1999. Neonatal Borna disease virus infection in the rat causes a loss of Purkinje cells in the cerebellum. *J. Neurovirol.* 5:181–189.
68. Weissenbock, H., M. Hornig, W.F. Hickey, and W.I. Lipkin. 2000. Microglial activation and neuronal apoptosis in Bornavirus infected neonatal Lewis rats. *Brain Pathol.* 10:260–272.
69. Sauder, C., and J.C. de la Torre. 1999. Cytokine expression in the rat central nervous system following perinatal Borna disease virus infection. *J. Neuroimmunol.* 96:29–45.
70. Ye, P., W. Price, G. Kassiotis, G. Kollias, and A.J. D'Ercole. 2003. Tumor necrosis factor-alpha regulation of insulin-like growth factor-I, type 1 IGF receptor, and IGF binding protein expression in cerebellum of transgenic mice. *J. Neurosci. Res.* 71:721–731.
71. Corbin, J.G., D. Kelly, E.M. Rath, K.D. Baerwald, K. Suzuki, and B. Popko. 1996. Targeted CNS expression of interferon-gamma in transgenic mice leads to hypomyelination, reactive gliosis, and abnormal cerebellar development. *Mol. Cell. Neurosci.* 7:354–370.
72. Ma, Q., D. Jones, P.R. Borghesani, R.A. Segal, T. Nagasawa, T. Kishimoto, R.T. Bronson, and T.A. Springer. 1998. Impaired B-lymphopoiesis, myelopoiesis, and derailed cerebellar neuron migration in CXCR4- and SDF-1-deficient mice. *Proc. Natl. Acad. Sci. USA.* 95:9448–9453.
73. Zou, Y.R., A.H. Kottmann, M. Kuroda, I. Taniuchi, and D.R. Littman. 1998. Function of the chemokine receptor CXCR4 in haematopoiesis and in cerebellar development. *Nature.* 393:595–599.
74. Wettschureck, N., and S. Offermanns. 2005. Mammalian G proteins and their cell type specific functions. *Physiol. Rev.* 85:1159–1204.
75. Boulanger, L., and M. Poo. 1999. Gating of BDNF-induced synaptic potentiation by cAMP. *Science.* 284:1982–1984.
76. Jouvenceau, A., G. Hedou, B. Potier, M. Kollen, P. Dutar, and I.M. Mansuy. 2006. Partial inhibition of PP1 alters bidirectional synaptic plasticity in the hippocampus. *Eur. J. Neurosci.* 24:564–572.
77. Brune, W., M. Hasan, M. Krych, I. Bubic, S. Jonjic, and U.H. Koszinowski. 2001. Secreted virus-encoded proteins reflect murine cytomegalovirus productivity in organs. *J. Infect. Dis.* 184: 1320–1324.
78. Johnson, K., L. Ryan, J. Davis, A. Elmore, B. Guenther, J. Marcus, and R.R. Maronpot. 2006. Application of magnetic resonance imaging in developmental neurotoxicity testing: a pilot study. *Neurotoxicology.* 27:846–851.
79. Van Tine, B.A., T.R. Broker, and L.T. Chow. 2005. Simultaneous in situ detection of RNA, DNA, and protein using tyramide-coupled immunofluorescence. *Methods Mol. Biol.* 292:215–230.
80. Nystrom, K., M. Biller, A. Grahn, M. Lindh, G. Larson, and S. Olofsson. 2004. Real time PCR for monitoring regulation of host gene expression in herpes simplex virus type 1-infected human diploid cells. *J. Virol. Methods.* 118:83–94.